Journal of Thermal Analysis and Calorimetry, Vol. 85 (2006) 3, 609–616

HYDRATION PROPERTIES OF SYMMETRIC CHAIN AND ASYMMETRIC CHAIN SPHINGOMYELIN BILAYERS

*Y. Kawasaki, A. Kuboki, S. Ohira and M. Kodama**

Department of Biochemistry, Faculty of Science, Okayama University of Science, 1-1 Ridai-cho, Okayama 700-0005, Japan

Hydration properties of lipid bilayer systems are compared for symmetric chain sphingomyelin (*N*-palmitoylsphingomyelin) and asymmetric chain sphingomyelin (*N*-lignoceroylsphingomyelin). These sphingomyelins were semisynthesized by a deacylation-reacylation process with a natural sphingomyelin used as a starting material. The number of differently bound water molecules was estimated by a deconvolution analysis of the ice-melting curves obtained by a differential scanning calorimetry (DSC) and was used to construct a water distribution diagram for these water molecules. Similarly to a natural sphingomyelin used for comparison, the asymmetric chain sphingomyelin was found to form small size vesicles having an internal cavity and incorporate 15 water molecules per molecule of lipid into its cavity, in contrast with 5 H_2O/lipid for freezable interlamellar water observed for large size multilamellar vesicles formed by the symmetric chain sphingomyelin.

Keywords: *deconvolution analysis, ice-melting DSC curves, interlamellar water, large size multilamellar vesicle, small size vesicle, symmetric chain and asymmetric chain sphingomyelins*

Introduction

Recently (1997), a new concept for cell membrane bilayer structure has been proposed [1]. This is based upon a clustering of sphingolipids and cholesterol to form microdomains known as raft and/or caveola. In this regard, much attention of investigation has been paid to sphingolipids which are main constituents of the microdomains [2, 3].

The fundamental molecular structure of sphingolipids is a sphingosine and an amide-linked acyl chain. Focusing on their backbone different from a glycerol backbone for glycerolipids, since the early 1970's, structural and functional properties of the sphingolipids have been studied [4–21]. In these past studies, a sphingomyelin (SM), which is the most typical sphingophospholipid and has a phosphorylcholine headgroup, has been most frequently used. However, studies of the interaction of SM and water molecules remain rather poorly understood, although they are the subject of many investigations.

On the other hand, naturally occurring SMs have been found to exist in a variety of molecular species differing widely in acyl chain-length (ranging from 14 to 26 carbons), although the other sphingosine chain is fixed at mostly 18 carbons long [8–10, 22–26]. Accordingly, the SMs having an acyl chain longer than at least 20 carbons are present as an asymmetric molecular species. In this connection, we refer to the past studies reported by Shipley's group [14–16]. In these studies, the uptake of interlamellar water between bilayers has been reported to be almost the same for symmetric chain and asymmetric chain SMs. However, we have an objection to the result obtained by Shipley's group. This is due to a marked difference in vesicular form observed by us for the symmetric chain and asymmetric chain SMs [27]. On this basis, it would be expected that the hydration property of bilayers becomes different between the two types of sphingomyelins. From this viewpoint, in the present study, the number of interlamellar water molecules of the SM-water systems was estimated by a deconvolution analysis of ice-melting curves obtained by a differential scanning calorimetry (DSC) and was compared for the symmetric chain and asymmetric chain SMs.

Experimental

Materials

A bovine brain SM (BSM) was purchased from Sigma Chemical Co. (St. Louis, MO)(material has Lot number of 120K1580). Both carbon number and double bond number in the acyl chain of BSM was determined by a positive ion electrospray ionization mass spectroscopy (ESI/MS).

* Author for correspondence: kodama@dbc.ous.ac.jp

1388–6150/$20.00

Akadémiai Kiadó, Budapest, Hungary
Springer, Dordrecht, The Netherlands

Semisynthesis of the *N*-palmitoylSM (C16:0-SM) and *N*-lignoceroylSM (C24:0-SM)

The semisynthesis was performed by the following procedures: the BSM (~500 mg) obtained from Sigma Chemical Co. was dispersed in ~35 mL of 1N methanolic HCl. To depress the epimerization and complete the deacylation reaction, the dispersion was stirred at a temperature around 50 lower by 20°C than the usual temperature and over 80 h periods longer by four times than the usual reaction period, after which the solvent was removed by a rotary evaporation. The resultant precipitate was suspended in benzene and then evaporated by a rotary evaporation. This process was repeated at least three times to completely remove residual water and was then followed by a silicic acid column chromatography (chloroform/methanol 9:1 (*v*/*v*)). The eluted fractions were monitored by a thin-layer chromatography developed in chloroform/methanol/ammonium hydroxide 25:17:3 (*v*/*v*). The precursor product, lysosphingomyelin salt (sphingosylphosphocholine·HCl) was dissolved in dry chloroform and was then neutralized by passing over negative ion exchange resin (Rexyn I-300), in order to obtain the lysosphingomyelin. The epimerization of the *D-erythro*-lysosphingomyelin into the *L-threo* configuration was checked to be less than 10% by ^{1}H–, and ^{13}C–NMR spectroscopies. The composition of a sphingosine chain for the resultant lysosphingomyelin was examined with the ESI/MS and ^{1}H–, and ^{13}C–NMR spectroscopies, showing that more than 95% of the total sphingosine chains were 18 carbons with a trans double bond at the C–4 position [13].

The reacylation procedures are performed as follows: The lysosphingomyelin dissolved in dry chloroform was reacylated with fatty acids having desired acyl chains in the presence of dicyclohexylcarbodiimide (DCC), respectively. The final products of C24:0-SM and C16:0-SM were purified by the silicic acid column chromatography developed in chloroform/methanol changing in *v*/*v* from 9:1 to 1:7. The purification was repeated up to at least three times until no changes in the gel-to-liquid crystal phase transition peak were observed by a DSC. Finally, the purity of three products was checked to be ~99% by a combination of thin-layer chromatography, high performance liquid chromatography, and ESI/MS. The overall yields for this semisynthesis achieved in 4 steps were ~30%.

Sample preparations for DSC

For a DSC, series of respective samples of the C16:0-SM-, C24:0-SM-, and BSM-water systems were prepared by varying water content as follows: The lipid (approximately 20 mg) in a high pressure crucible cell for a Mettler DSC apparatus was dehydrated under high vacuum (10^{-4} Pa) at room temperature for at least 3 days until no mass loss was detected by electroanalysis (Cahn Electrobalance). The crucible cell containing the dehydrated lipid was sealed off in a dry box filled with dry N_2 gas and was then weighed with a microbalance. The lipid-water samples of varying water contents were prepared by successive additions of the desired amounts of water to the same dehydrated SM (19.7 mg in mass) with a microsyringe. Thus, only the mass of water was changed throughout the preparation of series of samples. All the samples were weighed after each addition of water and were annealed with a Mettler calorimeter by repeating thermal cycling (scanning rate of 0.5°C min^{-1}) at temperatures above and below the gel-to-liquid crystal phase transition until the same lipid transition peak was attained. After the annealing, the loss of water in the samples was checked with the microbalance.

Sample preparations for electron microscopy

Vesicle dispersions of C16:0-SM, C24:0-SM, and BSM used for a negative stain electron microscopy were prepared according to a Bangham method [28], respectively: A lipid film was first prepared by removing chloroform from the lipid stock solution on a rotary evaporator, and then under high vacuum (10^{-4} Pa) to achieve complete removal of traces of the solvent. The resultant dried lipid film was dispersed in distilled water at a lipid concentration of ~2 mM and at temperatures of the liquid crystal phase, after which the dispersion was annealed with a temperature-controlled water bath by repeating thermal cycling at temperatures below and above the gel-to-liquid crystal phase transition to ensure complete suspension of the lipid. The vesicle preparations of respective SMs were prepared as follows: A drop of the dispersion thus obtained was placed on copper grids covered with carbon-coated collodion films, allowed to remain until attaining almost dry, after which a drop of 2% solution of sodium phosphotungstate (pH approximately 7) used as a stainer was added and the excess solution was then drained, followed by complete dry.

Instrumental methods

Differential scanning calorimetry (DSC)

DSC was performed with a Mettler TA-4000 apparatus for respective samples of the C16:0-SM-, C24:0-SM-, and BSM-water systems in the high pressure crucible cell (pressure resistant to 10 MPa) and

on heating from –70°C to a temperature of the liquid crystal phase at a rate of 0.5°C min^{-1}. The DSC was initiated by cooling the sample from a liquid crystal temperature directly to –70°C.

Electron microscopy

All the preparations of vesicles prepared according to the method described above (Sample preparation for electron microscopy) were supplied immediately to an electron microscopy. The electron microscopy was carried out with a JEOL JEM-2000EX and a Hitachi H-8100 at around 20°C of a room temperature.

Electrospray ionization mass spectrometry (ESI/MS) for naturally occurring BSM and synthesized SMs

An acyl chain composition of the natural BSM was determined by ESI/MS (JEOL, Japan) [24–26]. Furthermore, the ESI/MS was used to check the purity of the semisynthesized SMs. The positive ESI mass spectrum of respective SM molecular species was measured for a molecular ion adduct found as $[SM+Na]^+$ ($[SM+23]^+$) and was used to calculate both the total carbon number and the total double bond number given by two chains, sphingosine and amide-linked acyl chains. Next, the carbon number and the double bond number in the acyl chain alone were calculated by assuming that the sphingosine chain of respective SM molecular species is all C18:1. In Table 1, the molecular species detected for the natural BSM are shown by the carbon number and the double bond number of their acyl chain, together with their composition estimated from the relative intensity of mass spectrum. The average molecular mass of the BSM used in the present study was estimated to be 772.

Table 1 SM molecular species and their acyl chain composition obtained by an electrospray ionization mass spectrometry (ESI/MS) for naturally occurring bovine brain sphingomyelin

CN:DBN[(a)] for amide-linked acyl chain	composition /mol%
14:0	0.0
14:1	0.0
16:0	3.3
16:2	0.0
17:0	0.0
18:0	39.4
19:0	0.7
20:0	6.0
20:2	0.0
21:0	1.3
22:0	2.0
22:1	0.0
23:0	2.7
24:0	12.4
24:1	31.5
24:2	0.8

[(a)]Total carbon number (CN): total double bond number (DBN) for amide-linked acyl chains estimated with a sphingosine chain C18:1

Analysis of ice-melting DSC curves

A deconvolution analysis was performed with a computer program for multiple Gaussian curve analysis (ORIGIN, Microcal Software, Inc.) to separate the ice-melting DSC curves into two components, broad and sharp, for freezable interlamellar water (i.e., existing in regions between lipid bilayers) and bulk water (i.e., existing outside the bilayers), respectively, because the two components overlap at their bases. Furthermore, the component of freezable interlamellar water was deconvoluted into multiple components. The deconvolution was performed under the following conditions: the number of deconvoluted components was minimized until a theoretical curve is best fitted to an experimental DSC curve, and both a half-height width and a midpoint temperature characteristic of each deconvoluted curve were maintained almost constant throughout all the deconvolutions for varying water contents [29–31].

Estimation of the numbers of freezable water molecules

Ice-melting enthalpies of individual deconvoluted curves were used to estimate respective average molar ice-melting enthalpies for freezable interlamellar and bulk water [30, 31]. The number of freezable interlamellar water molecules (*NF*) per molecule of lipid at a desired water content is given by

$$N_F = \sum_i \Delta H_F(i) / \Delta H_F^a \quad (1)$$

where $\Delta H_F(i)$ [i=I, II,..., N] is the ice-melting enthalpy of deconvoluted component i for the freezable interlamellar water per mole of lipid, and so $\Delta H_F(i)$ gives the total ice-melting enthalpy per mole of lipid for this type of water. ΔH_F^a is the average ice-melting enthalpy per mole of water present as the freezable interlamellar water and is given by a slope of linear curve obtained by a plot of $\sum_i \Delta H_F(i)$ *vs.* N_w expressed in the water/lipid molar ratio.

The number of bulk water molecules (N_B) per molecule of lipid was estimated from $\Delta H_B/\Delta H_B^a$,

where ΔH_B is the ice-melting enthalpy of deconvoluted bulk component per mole of lipid. The average ice-melting enthalpy (ΔH_B^a) per mole of water present as the bulk water was likewise obtained from a slope of the ΔH_B *vs*. N_w linear curve.

Results and discussion

The three systems of the C16:0-SM-, C24:0-SM-, and BSM-water show a phase transition behavior commonly observed for lipid-water systems [29–31]. For an example, Fig. 1 shows a series of typical DSC curves of varying water contents obtained for the C16:0-SM-water system. In this figure, the ice-melting peaks observed at low temperatures are followed by lipid transition peaks of the gel-to-liquid crystal phase at high temperatures. Accordingly, all the ice-melting peaks shown in Fig. 1 are derived from freezable water molecules existing in the gel phase. In Fig. 2, a series of the ice-melting DSC curves of varying water contents obtained for the C16:0-SM-water system is shown in an enlarged scale. In this figure, the ice-melting DSC curves are shown to be comprised of two components, broad (a wide temperature range of –40 to about 0°C) and sharp (a narrow temperature range around 0°C), for the freezable interlamellar and bulk water, respectively [29–31]. Since the sharp ice-melting peak for the bulk water is situated at around 0°C, the structure of ice for the bulk water is suggested to be close to that of the most ordered hexagonal ice for free water. While the broad ice-melting DSC curve for the freezable interlamellar water suggests that the ice of this type of water is present in plural structures far different from the hexagonal ice [31].

A deconvolution analysis was performed to separate the ice-melting DSC curves into the two compo-

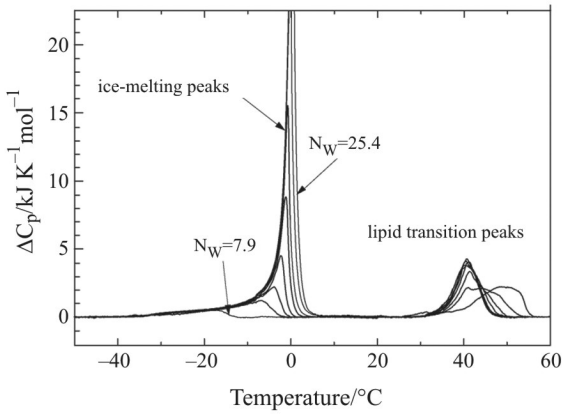

Fig. 1 A series of DSC curves for the gel phase of the C16:0-SM-water system ranging in the water/lipid molar ratio (N_w) from 7.9 to 25.4

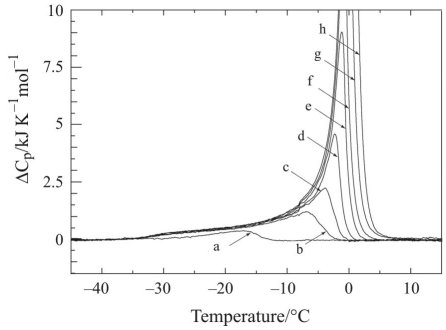

Fig. 2 A series of ice-melting DSC curves for the gel phase of the C16:0-SM-water system at varying water contents expressed in the water/lipid molar ratios (N_w) of a – 7.9, b – 9.2, c – 10.5, d – 12.1, e – 14.2, f – 16.7, g – 20.6, h – 25.4

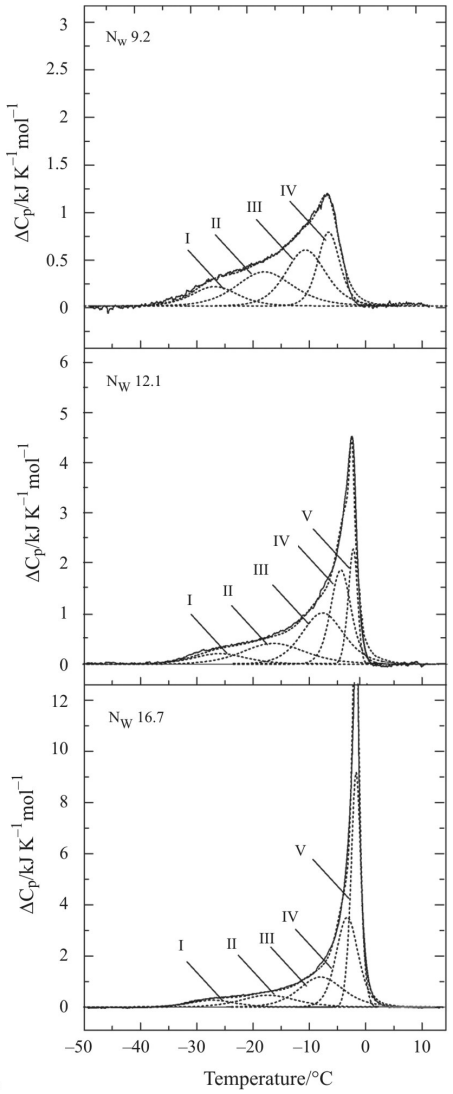

Fig. 3 Deconvolution analysis of ice-melting DSC curves for the gel phase of the C16:0-SM-water system at the water/lipid molar ratios (N_w) of a – 9.2, b – 12.1 and c – 16.7. The deconvoluted curves I-V and their sum (the theoretical curve) are shown by dotted lines, and the experimental DSC curves are represented by solid lines

nents as accurately as possible. In Fig. 3, typical results of the deconvolution analysis for the C16:0-SM-water system are compared for varying water contents at N_w values of 9.2 (a), 12.1 (b) and 16.7 (c). As shown in Figs 3b and c, the broad ice-melting peak for the freezable interlamellar water was finally deconvoluted into four components, I, II, III, and IV, which successively appear with increasing water content. So, four deconvoluted components obtained for the broad ice-melting peaks suggest that on cooling the freezable water molecules existing in regions between the lipid bilayers form at least four types of ice differing in the mode of their hydrogen bonding. Presumably, the ice formed by the freezable interlamellar water molecules is more remote from the bilayer surfaces in the order of components I, II, III and IV [31]. On the other hand, a single deconvoluted component V observed in Figs 3b and c for N_w values of 12.1 and 16.7 is assigned to the bulk water.

For the C16:0-SM-water system, the ice-melting enthalpy for the freezable interlamellar water, $\sum_i \Delta H_F\,(i)$, given in Eq. (1) was obtained by the sum of respective ice-melting enthalpies of deconvoluted components I, II, III, and IV. The resultant $\sum_i \Delta H_F\,(i)$ was plotted *vs*. N_w. The result for the C16:0-SM-water system is shown in Fig. 4a. In this figure, the ice-melting enthalpy ΔH_B for the bulk water obtained from the deconvoluted component V is compared. The same deconvolution analysis was applied to the C24:0-SM-, and BSM-water systems. Figures 4b and c show the results for the C24:0-SM-, and BSM-water systems, respectively. In Fig. 4, all the systems show a specific region previously reported by us for glycerophospholipid-water systems [29–31]. In this region, the bulk water appears although the limiting, maximum amount of freezable interlamellar water is not yet reached. However, the $\sum_i \Delta H_F\,(i)$ curve of the three systems shows a linear curve characterized only by the freezable interlamellar water at water contents lower than the specific region, so that its slope obtained by a least square method gave the average molar ice-melting enthalpy for the freezable interlamellar water. By applying such estimation, the molar ice-melting enthalpy for the bulk water was obtained for the three systems because a linear ΔH_B curve characterized only by the bulk water is observed for these systems at water contents higher than the specific region. Table 2 shows the average molar ice-melting enthalpies for the freezable interlamellar (ΔH_F^a) and bulk water (ΔH_B^a) of the three systems,

Table 2 Average molar ice-melting enthalpies for freezable interlamellar (ΔH_F^a) and for bulk water (ΔH_B^a) of the C16:0-SM, C24:0-SM, and BSM systems

	Average molar ice-melting enthalpy /kJ mol^{-1} H_2O	
	ΔH_B^a	ΔH_F^a
C16:0-SM-water	5.90	5.06
C24:0-SM-water	5.94	5.40
BSM-water	5.94	5.44
free water	6.01	

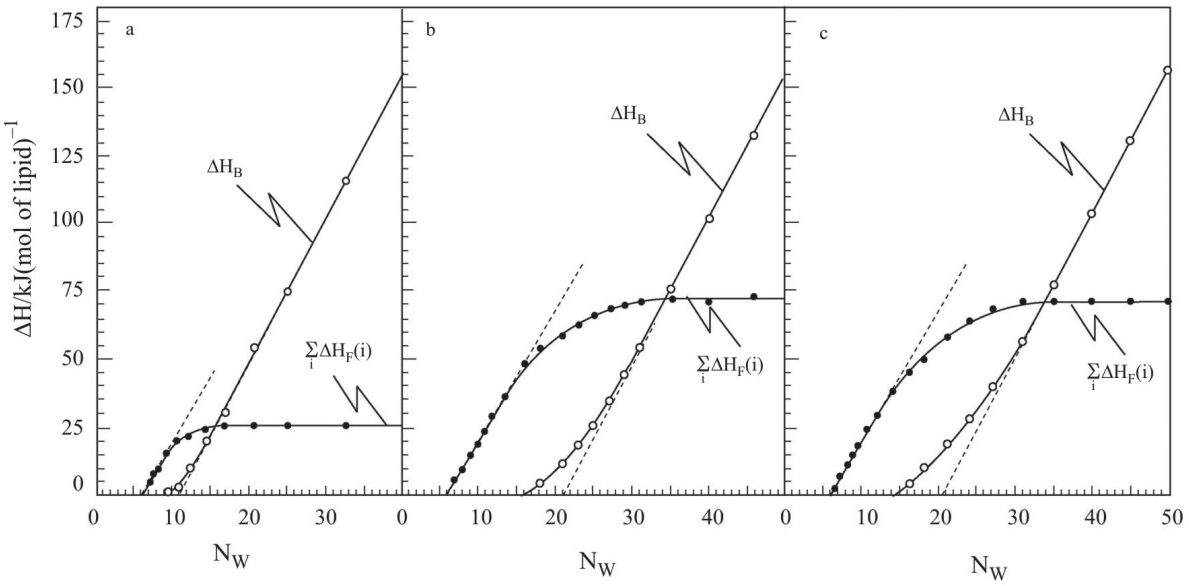

Fig. 4 Ice-melting enthalpy for freezable interlamellar water ($\sum_i \Delta H_F$(i)) is plotted the water/lipid molar ratio (N_w) for the gel phase of a – C16:0-SM, b – C24:0-SM, and c – BSM systems. For comparison, ice-melting enthalpy for bulk water (ΔH_B) is also plotted *vs*. N_w. Linear $\sum_i \Delta H_F(i)$ and ΔH_B curves obtained by a least squares method are extrapolated by dashed lines, respectively

respectively. As show in this table, the ΔH_F^a values for the C24:0-SM and BSM systems are larger than that for the C16:0-SM system although the ΔH_B^a value is almost the same for the three systems.

According to Eq. (1), the number of freezable interlamellar water molecules per molecule of lipid for the three systems was calculated from the respective average molar ice-melting enthalpies (ΔH_F^a) shown in Table 2. Similarly, the number of bulk water molecules per molecule of lipid was estimated with the average ice-melting enthalpy (ΔH_B^a) shown in Table 2.

On the other hand, in Fig. 4, all the linear $\sum_i \Delta H_F(i)$ curves of the three systems were shown to intersect the abscissa just at N_w 6. This indicates that all the water added up to N_w 6 is unable to form ice-like structure even when cooled to extremely low temperatures (–70ºC) and is present as non-freezable interlamellar water. The non-freezable water molecules are considered to be confined within narrow regions between adjacent lipid headgroups and form their hydrogen bonding to a hydroxyl and an amide group of the SM molecules. Therefore, the limiting, maximum number of non-freezable interlamellar water molecules becomes the same, 6 H_2O/lipid, for the three systems because the three SMs have the same functional groups acting as a hydrogen bond donor and acceptor. In Fig. 5, the cumulative numbers of non-freezable interlamellar, freezable interlamellar, and bulk water molecules per molecule of lipid are plotted *vs*. N_w for the C16:0-SM (a), C24:0-SM (b) and BSM systems (c). In this figure, a drastic difference is observed for the number of freezable interlamellar water molecules. Thus, the limiting number of this freezable water molecules for the C24:0-SM and BSM systems reaches 15 H_2O/lipid and 14.5 H_2O/lipid, respectively, and is approximately 2.7 times larger than that (5.5 H_2O/lipid) for the C16:0-SM system. On the basis of this difference, a negative stain electron microscopy was performed to obtain structural information of the vesicles of C16:0-SM, C24:0-SM, and BSM. In Fig. 6, the electron micrographs are compared for the C16:0-SM (a), C24:0-SM (b) and BSM (c). For the C16:0-SM shown in Fig. 6a, fairly large size multilamellar vesicles are observed and their size is more than 4 μm in diameter. In this contrast, the micrographs for the respective vesicles of C24:0-SM and BSM show only small size vesicles (100~200 nm in diameter) having an internal cavity surrounded by one or more lamellae. In our previous paper [27], we have already reported the characteristic property of the asymmetric chain length SM that is its ability to form small size vesicles of a highly curved surface, in contrast with large size multilamellar vesicles formed by the symmetric chain length SM. In this connection, it has been reported by X-ray diffraction studies [16, 17] that the asymmetric chain C24:0-SM adopts a partially interdigitated packing arrangement in the gel state in such a way that the shorter sphingosine chain of lipid in one monolayer pack, end to end, with the longer acyl chain of another lipid in opposite monolayer of the bilayer. Furthermore, the terminal methyl groups of two chains of the asymmetric SM have been reported to undergo a rotational motion, even in the gel state. Such a motion for the terminal end of the shorter sphingosine chain would induce kinked conformations of the longer acyl chain [6, 32, 33]. The resultant kinked acyl chain would make it possible for the C24:0-SM molecule to adopt both a truncated corn (outer monolayer) and an inverted truncated corn shape (inner monolayer) which are required to form a highly

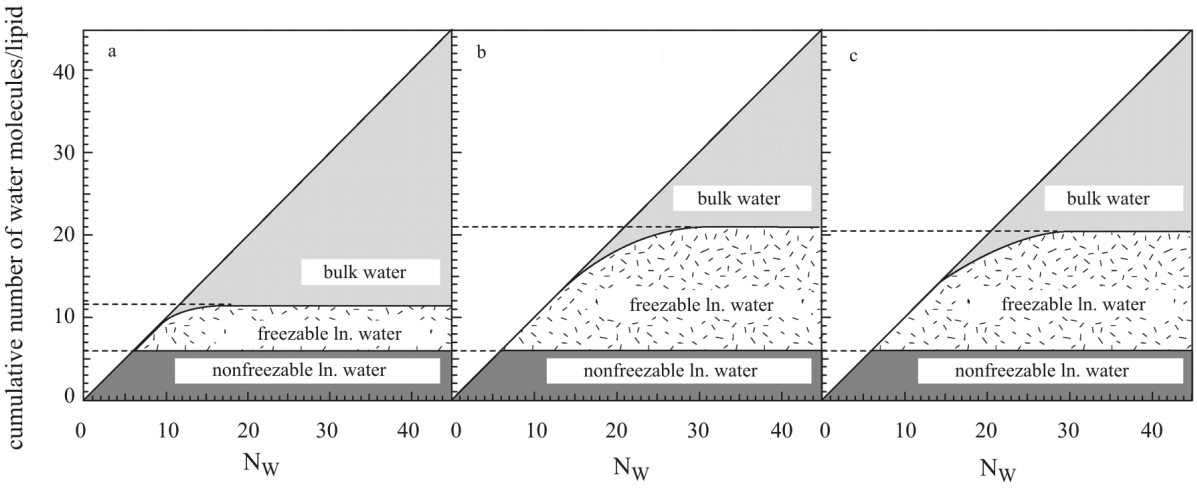

Fig. 5 Water distribution diagram for the gel phase of a – C16:0-SM b – C24:0-SM, and c – BSM systems. The cumulative numbers of water molecules (per molecule of lipid) present as non-freezable interlamellar and freezable interlamellar water and as bulk water are plotted *vs*. the water/lipid molar ratio (N_w)

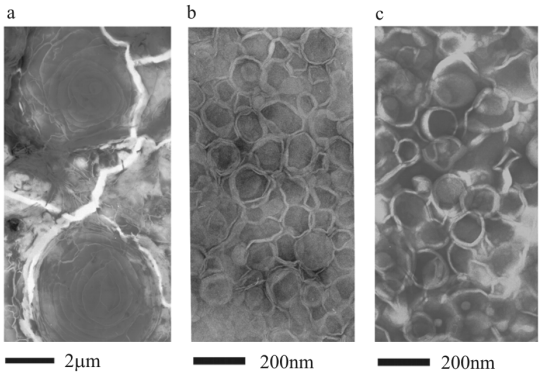

Fig. 6 Negative stain electron micrographs for the vesicles of a – C16:0-SM, b – C24:0-SM and c – BSM

curved surface characteristic of small size vesicles [34, 35]. Accordingly, as shown in Fig. 6c, the BSM used in the present study also forms the small size vesicles similar to those of the C24:0-SM because the natural SM contains asymmetric chain molecular species up to 50 mol% (Table 2).

Here, we focus on the internal cavity observed for the small size vesicles of the C24:0-SM and BSM. The cavity incorporates water molecules in its inside and forms the so-called water pool. When compared at the same lipid concentration of 2 mM used in the electron microscopy, the amount of water incorporated into the cavity is calculated to be at least 10 times larger than that of water incorporated into narrow interlamellar spaces of large multilamellar vesicles. This calculation was made by assuming that the diameters of the small unilamellar vesicle and the large multilamellar vesicle are 150 nm and 4 μm, respectively, and the multilamellar vesicle is composed of fifteen stacked lamellae. Such a large volume for the cavity results in the large uptake of freezable interlamellar water for the small vesicles of C24:0-SM and BSM observed in the present study. However, there is some question as to whether all the water molecules incorporated into the cavity behave as freezable interlamellar water. Presumably, the cavity water molecules approach more closely bulk water the more remote the water molecules are from the bilayer surfaces composed of the phosphorylcholine polar headgroups present as dipolar zwitterions. So, as shown in Table 2, the average molar ice-melting enthalpy for the freezable cavity water molecules of the C24:0-SM and BSM vesicles is larger than that for the freezable interlamellar water molecules of the C16:0-SM vesicle and is closer to the melting enthalpy of hexagonal ice, 6.01 kJ mol^{-1} water.

Acknowledgements

This work is supported in part by Grants-in-Aid for General Scientific Research (15550133) from Ministry of Education, Science and Culture, Japan (2003), and by 'High-Tech Research Center' Project for Private Universities: matching fund subsidy from MEXT (Ministry of Education, Culture, Sports, Science and Technology).

References

1 K. Simons and E. Ikonen, Nature, 387 (1997) 569.
2 A. Prinetti, V. Chigorno, G. Tettamanti and S. Sonnino, J. Biol. Chem., 275 (2000) 11658.
3 U. Ortegren, M. Karlsson, N. Blazic, M. Blomqvist, F. H. Nystrom, J. Gustavsson, P. Fredman and P. Stralfors, Eur. J. Biochem., 271 (2004) 2028.
4 L. K. Bar, Y. Barenholz and T. E. Thompson, Biochemistry, 36 (1997) 2507.
5 T. N. Estep, W. I. Calhoun, Y. Barenholz, G. G. Shipley and T. E. Thompson, Biochemistry, 19 (1980) 20.
6 I. W. Levin, T. E. Thompson, Y. Barenholz and C. Huang, Biochemistry, 24 (1985) 6282.
7 R. Cohen, Y. Barenholz, S. Gatt and A. Dagan, Chem. Physis. Lipids, 35 (1984) 371.
8 Y. Barenholz, J. Suurkuusk, D. Mountcastle, T. E. Thompson and R. L. Biltonen, Biochemistry, 15 (1976) 2441.
9 W. I. Calhoun and G. G. Shipley, Biochim. Biophys. Acta, 555 (1979) 436.
10 S. H. Untracht and G. G. Shipley, J. Biol. Chem., 252 (1977) 4449.
11 P. R. Maulik, D. Atkinson and G. G. Shipley, Biophys. J., 50 (1986) 1071.
12 G. G. Shipley, L. S. Avecilla and D. M. Small, J. Lipid Res., 15 (1974) 124.
13 P. K. Sripada, P. R. Maulik, J. A. Hamilton and G. G. Shipley, J. Lipid Res., 28 (1987) 710.
14 P. R. Maulik, P. K. Sripada and G. G. Shipley, Biochim. Biophys. Acta, 1062 (1991) 211.
15 P. R. Maulik and G. G. Shipley, Biochemistry, 35 (1996) 8025.
16 P. R. Maulik and G. G. Shipley, Biophys. J., 69 (1995) 1909.
17 T. J. McIntosh, S. A. Simon, D. Needham and C. Huang, Biochemistry, 31 (1992) 2020.
18 D. A. Mannock, T. J. McIntosh, X. Jiang, D. F. Covey and R. N. McElhaney, Biophys. J., 84 (2003) 1038.
19 Xin-Min Li, M. M. Momsen, H. L. Brockman and R. E. Brown, Biophys. J., 85 (2003) 3788.
20 Xin-Min Li, J. M. Smaby, M. M. Momsen, H. L. Brockman and R. E. Brown, Biophys. J., 78 (2000) 1921.
21 J. M. Smaby, V. S. Kulkarni, M. Momsen and R. E. Brown, Biophys. J., 70 (1996) 868.
22 D. Marsh, CRC Handbook of Lipid Bilayers, CRC Press, Boca Raton FL, 1990, pp. 68–70.
23 R. Koynova and M. Caffrey, Biochim. Biophys. Acta, 1255 (1995) 213.
24 J. L. Kerwin, A.R. Tuininga and L.H. Ericsson, J. Lipid Res., 35 (1994) 1102.

25 W. Pruzanski, E. Stefanski, F. C. de Beer, M. C. de Beer, A. Ravandi and A. Kuksis, J. Lipid Res., 41 (2000) 1035.
26 A. A. Karlsson, P. Michelsen and G. Odham, J. Mass Spectrom., 33 (1998) 1192.
27 Y. Kawasaki, A. Kuboki, S. Ohira and M. Kodama, Thermochim. Acta, 431 (2005) 188.
28 A. D. Bangham, M. W. Hill and N. G. A. Miller, Methods Membr. Biol., 1 (1974) 1.
29 M. Kodama, H. Aoki, H. Takahashi and I. Hatta, Biochem. Biophys. Acta, 1329 (1997) 61.
30 M. Kodama, Y. Kawasaki, H. Aoki and Y. Furukawa, Biochim. Biophys. Acta, 1667 (2004) 56.
31 M. Kodama and H. Aoki, Water behavior in phospholipid bilayer systems, in: N. Garti (Ed.), Surfactant Science Series 93, Thermal Behavior of Dispersed Systems, Marcel Dekker, New York, 2000, pp. 247–293.
32 P. G. Barton and F. D. Gunstone, J. Biol. Chem., 250 (1975) 4470.
33 J. T. Mason, Ching-hsien Huang and R. L. Biltonen, Biochemistry, 20 (1981) 6086.
34 R. N. A. H. Lewis, D. A. Mannock and R. N. McElhaney, Membrane Lipid Molecular Structure and Polymorphism, in: R. Epand (Ed.), Current Topics in Membranes, Vol. 44, Lipid Polymorphism and Membrane Properties, Academic Press, 1997, pp. 25–81.
35 C. Hang and J. T. Mason, Proc. Natl. Acad. Sci., USA, 75 (1978) 308.

DOI: 10.1007/s10973-006-7659-2